DETC2003/VIB-48358

A TECHNIQUE FOR VALIDATING A MULTIBODY WHEEL/RAIL CONTACT ALGORITHM

José L. Escalona
Department of Mechanical and Materials Engineering
University of Seville
Camino de los Descubrimientos s/n,
41092, Seville, Spain

Manuel González
Laboratorio de Ingeniería Mecánica
Escuela Politécnica Superior
University of La Coruña
Mendizábal s/n,
15403, Ferrol, Spain

Khaled E. Zaazaa
Ahmed A. Shabana
Department of Mechanical Engineering
University of Illinois at Chicago
842 West Taylor Street
Chicago, Illinois 60607-7022
Email: kzaaza1@uic.edu

ABSTRACT

In this paper, a specialized steady state formulation is developed in order to validate the results obtained using multibody wheel/rail two-point contact algorithms developed at the University of Illinois at Chicago. In the specialized formulation, the wheel set is assumed to have three points of contact with the rail. The steady state curving behavior of the wheel set is examined using this specialized formulation. The balanced steady state curving behavior in which the centrifugal force is equal to the lateral component of the gravity force can be obtained as a special case of the specialized steady state formulation developed in this investigation. No derailment analysis or scenarios are considered in this paper in order to validate the results of both the constraint and elastic contact formulations. The results of the simple specialized formulation are compared with the results of the multibody inverse and forward dynamics approaches. In the inverse dynamics, approach it is assumed that the wheel set will maintain three points of contact with the rail. The inverse dynamics formulation model is conceptually different from the specialized steady state formulation since in the inverse dynamics all the degrees of freedom are specified. In the multibody forward dynamics method, no assumptions are made with regard to the existence of the flange contact.

1. INTRODUCTION

In the railroad vehicles, one of the most important scenarios is the curve negotiation. In this scenario the wheels, as shown in Fig. 1, can experience two-point contact due to the centrifugal forces, and also due to yaw and hunting motion. However, the forces acting at the flange of the wheels and the gage face of the rails can be much larger than the centrifugal forces. The analysis of these forces is important for two main reasons:

1. Existing derailment criteria are functions of the ratio between the lateral and the vertical components of the contact forces. It is known that if the lateral contact force on the flange becomes sufficiently high the wheel climbs the rail and the possibility of derailment increases. Nadal [1] used a simple equilibrium of forces on the inclined plane of contact between wheel and rail to define the ratio of the lateral and vertical components of the contact forces. This ratio is a function only of the flange angle and the flange coefficient of friction.

2. Tangential forces at the flange contact due to sliding lead to an increase in the longitudinal tangential force at the tread. This is a consequence of the friction theory provided that there is no gross sliding at the tread. The tangential forces are source of high energy dissipation and wear of the wheels.

Elkins and Weinstock [2] demonstrated the need for including the two-point contact in the analytical study of curving behavior. In their investigation, four analytical methods were used to study the curving behavior. The analytical results were compared with the results obtained from a series of tests sponsored by the Urban Mass Transportation Administration (UMTA). Elkins and Weinstock concluded that the analytical methods that assume single point contact lead to significant

errors in predicting curving behavior when two-point contact occurs. In an earlier investigation, Boockock [3] developed expressions for the creepages for the quasi-static linear case. In order to include the effect of wheel-rail cross sectional geometry, Elkins and Gostling [4] used a quasi-static curving theory to improve the creepage expressions given by Boockock. The new expressions account for wheel-rail large contact angle that is expected in case of curve negotiations. Garg and Dukkitapi [5] presented one model of freight cars based on the work of Nagurka et al. [6], and two models for locomotive/passenger cars to analyze steady state curving behavior. The first model for locomotive/passenger cars employed the friction center method, developed by Smith et al. [7]. This model, however, does not account for some important design and operation parameters. In order to account for different suspension designs, the direct formulation [8] was also presented in [5]. Dukkitapi and Swamy [9] developed a new model to analyze the curving behavior of railway trucks with independently rotating wheel sets (IRW). To predict the wheel-rail forces in curving, non-linear wheel-rail geometry and non-linear creep-force models (heuristic method [5]) were used. Meinke and Blenkle [10] demonstrated numerically and experimentally the instabilities that occur during the narrow curve negotiation of wheel sets. These instabilities are due to self-excited coupled bending/torsion vibrations of the wheel set and lead to corrugation of the inner rail.
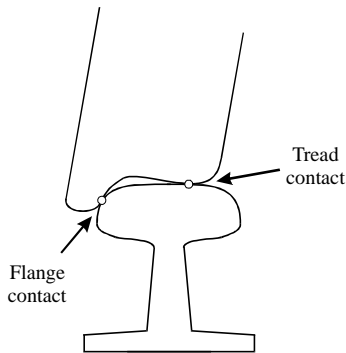

Figure 1. Two-point contact in wheel/rail interaction.

Steady State Curving Behavior   Simulation results of the motion of a single wheel set on a curved track [11] show that the wheel on the outer rail can have two points of contact; and in some motion scenarios, the wheel set maintains constant roll and yaw angles. Figure 2 shows the roll and yaw angles of a wheel set that travels with a velocity of 10 m/s on a track with 5 deg curvature. The results of this simulation are obtained assuming a coefficient of friction equal to 0.5. It can be observed that after the flange of the right wheel comes into contact with the rail, the roll and yaw angles remain approximately constant. In this paper, this scenario is referred to as *steady state curving behavior* [2], although some authors consider the steady state curving behavior as the case in which the wheel set centrifugal force balances the lateral component of the gravity force. This special case of balanced steady state curving behavior which can be difficult to precisely achieve in practice can be obtained as a special case of the formulations developed in this paper. Shabana et al. [11] presented the forces that act on the wheel set. It was shown that the contact force on the flange of the right wheel is more than ten times larger than

the centrifugal force. This result shows clearly the difference between the steady state curving behavior examined in this paper and the steady state curving behavior discussed by other authors.
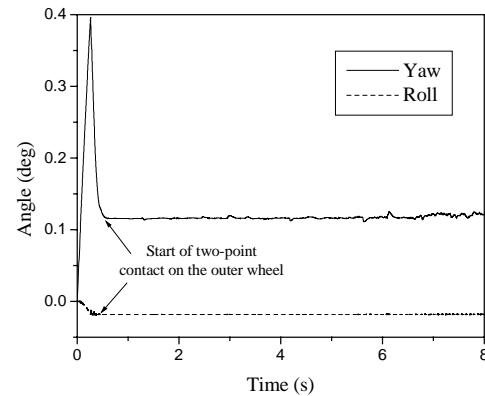

Figure 2. Roll and yaw angles.

Organization and Scope of this Study   The objective of this paper is to present a new technique for validating a multibody wheel/rail contact algorithm. This technique is based on a detailed study of the problem of the two-point contact in railroad vehicle dynamics during curve negotiation. To this end, the steady state equilibrium configurations, the inverse dynamic and forward dynamic analysis of the steady state curving behavior of the wheel sets are examined. Specifically, the following three different methods are used in this investigation:

1. *Steady State Equilibrium Analysis*. A dynamic problem of a wheel set negotiating a curved track is formulated using an analytical approach. In the model used, it is assumed that the wheel set has three points of contact with the rails (tread and flange contacts for the right wheel, and tread contact for the left wheel). By specifying the forward velocity of the wheel set and assuming that the yaw angle and the wheel set angular velocity about its axis are constant, a dynamic problem can be formulated using a set of algebraic equations. The resulting dynamic equilibrium problem, that does not require the use of the methods of numerical integration, is solved for the position and orientation of the wheel set, the wheel set angular velocity and the contact and driving forces as function of the wheel set forward velocity, the track curvature and the track superelevation. In this approach kinematic constraints are used for all contacts.

2. *Inverse Dynamic Solution Using Multibody System Algorithms*. An inverse dynamic problem is solved using general-purpose multibody system algorithms. However, in this method, the yaw angle and angular velocity of the wheel set are constrained, using the values obtained from the results of the previous method. All contacts are modeled using kinematic constraints [15,16]. The technique of Lagrange multipliers is used to predict the normal contact forces. In this method, the forward velocity, yaw angle and wheel set angular velocity are specified. These three constraints with the assumption of three contacts eliminate all degrees of freedom of the wheel set.

3. *Dynamic Analysis Using General Multibody Algorithms*. In the third method used in this investigation, the yaw angle

and wheel set angular velocity are not constrained. This forward dynamic problem requires the use of numerical integration to obtain the solution of the equations of motion. The wheel set model is analyzed in this investigation using general-purpose multibody system algorithms that can employ Lagrange multipliers or an elastic contact force model to determine the normal contact forces [11].

The numerical results using these three different methods are compared. The effect of the flange contact on the forces at the tread contact is also demonstrated. The analysis and results presented in this paper demonstrate the feasibility of using general-purpose multibody computer programs to predict the dynamics of railroad vehicles during curve negotiations.

This paper is organized as follows. Section 2 explains the coordinates and frames of reference used in the kinematic description of the wheels and rails. Section 3 describes the assumptions and details of the specialized analytical formulation used in the first method of the steady state equilibrium analysis. Section 4 provides a brief review of the multibody system formulations employed in the second and third methods for the simulation of the two-point contact problem. Section 5 provides the solution of the steady state equilibrium analysis. In Section 6, a comparison of the results obtained using different method is presented. In Section 7, summary and conclusions drawn from this study is presented.

2. GEOMETRY AND KINEMATIC DESCRIPTION

In the general formulation of the contact between a rigid wheel and a rigid rail, two surface parameters are used to describe the geometry of each of the two surfaces in contact. The two surface parameters s_1^r and s_2^r are used to describe the geometry of the rail surface, and s_1^w and s_2^w are the two surface parameters used to describe the wheel surface, as shown in Fig. 3. The position vector of a point on the wheel or the rail surfaces can be defined in the respective body coordinate system as

$$\overline{\mathbf{u}}^l = \overline{\mathbf{u}}^l(s_1^l, s_2^l) \qquad (1)$$

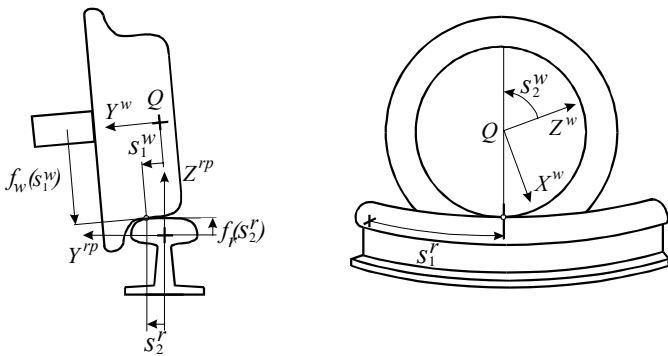where $l = w$ or r, and superscript w and r refer to wheel and rail, respectively.

Figure 3. Surface parameters.

Track Geometry Figure 4 shows a curved rail r with an arbitrary geometry and surface profile. The surface geometry of the rail r can be described in the most general case using the

two surface parameters s_1^r and s_2^r, where s_1^r represents the rail arc length and s_2^r is the surface parameter that defines the rail profile, as shown in Fig. 3. For convenience and simplicity, the surface parameter s_2^r is defined in a profile coordinate system $X^{rp}Y^{rp}Z^{rp}$, also shown in Figs. 3 and 4. The location of the origin and the orientation of the profile coordinate system, defined respectively by the vector $\mathbf{R}^{rp}$ and the transformation matrix $\mathbf{A}^{rp}$, can be uniquely determined using the surface parameter s_1^r [12]. Using this description, the global position vector of an arbitrary point on the surface of the rail r can be written as follows [11,12]:

$$\mathbf{r}^r = \mathbf{R}^{rp} + \mathbf{A}^{rp}\overline{\mathbf{u}}^{rp} \qquad (2)$$

where $\overline{\mathbf{u}}^{rp}$ is the local position vector that defines the location of the arbitrary point on the rail surface with respect to the profile coordinate system. Note that due to the above-mentioned description of the rail geometry, one has

$$\mathbf{R}^{rp} = \mathbf{R}^{rp}\left(s_1^r\right), \ \ \mathbf{A}^{rp} = \mathbf{A}^{rp}\left(s_1^r\right), \ \ \overline{\mathbf{u}}^{rp} = \begin{bmatrix} 0 & s_2^r & f_r\left(s_2^r\right) \end{bmatrix}^T \ \ (3)$$

where f_r is a function that defines the rail profile. In this investigation f_r can be defined analytically or using a spline function representation. The transformation matrix $\mathbf{A}^{rp}$ can be expressed in terms of three Euler angles, each of which can be expressed uniquely in terms of the surface parameter s_1^r [12].
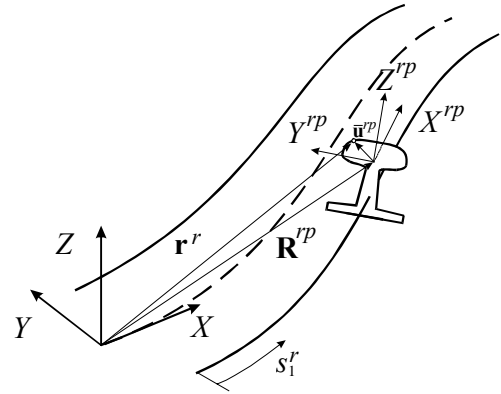

Figure 4. Track geometry.

Wheel Geometry Figure 5 shows a wheel set with an arbitrary surface profile. The surface geometry of the wheel w can be described using the two surface parameters s_1^w and s_2^w. The surface parameters are defined in a wheel set coordinate system $X^w Y^w Z^w$, also shown in the figure. The surface parameter s_1^w defines the wheel profile and s_2^w represents the angular surface parameter, as shown in Fig. 3. The location of the origin and the orientation of the wheel set coordinate system are defined, respectively, by the vector $\mathbf{R}^w$ and the transformation matrix $\mathbf{A}^w$. Using this description, the global position vector of an arbitrary point on the surface of the wheel w can be written as follows:

$$\mathbf{r}^w = \mathbf{R}^w + \mathbf{A}^w\overline{\mathbf{u}}^w \qquad (4)$$

where $\overline{\mathbf{u}}^w$ is the local position vector that defines the location of the arbitrary point on the wheel surface with respect to the wheel set coordinate system. In the case of the right wheel, this vector is defined as

$$\overline{\mathbf{u}}^w = \begin{bmatrix} f_w\left(s_1^w\right)\sin s_2^w & -L + s_1^w & f_w\left(s_1^w\right)\cos s_2^w \end{bmatrix}^T \quad (5)$$

where f_w is the function that defines the wheel profile, and L is the distance between the origin of the wheel set coordinate system and point Q of the wheel, as shown in Figs. 3 and 5. In this investigation f_w can be defined analytically or using a spline function representation.
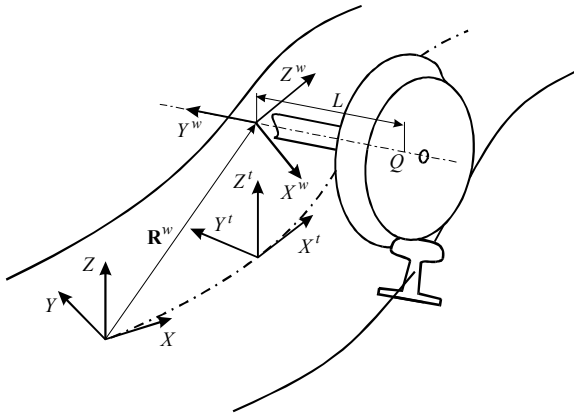

Figure 5. Wheel set position.

3. STEADY STATE EQUILIBRIUM ANALYSIS

In this section, a special case study of a wheel set traveling on a curved track is defined. The objective of introducing this problem is to have a better understanding of the nature of the contact forces when the wheel set moves on a curved track. The formulation of this dynamic equilibrium problem leads to a system of nonlinear algebraic equations that can be solved for the contact forces, driving forces and wheel set yaw angle and angular velocity as functions of the forward velocity, curvature and superelevation of the rails. The results obtained using the closed form equations of the resulting dynamic equilibrium problem are compared in section 6 with the results obtained using a general-purpose multibody computer code.

In addition to the coordinate systems previously defined, a track coordinate system $X^t \, Y^t \, Z^t$ shown in Fig. 5 is also used. The origin of the track coordinate system is located at the track center curve and is assumed to follow the forward motion of the wheel set. Axes X^t and Y^t are tangent and normal to the track curve, respectively. Figure 6 shows the position of the track coordinate system for a track with a constant curvature and no superelevation. In case of superelevation, the assumed orientation of the track coordinate system is shown in Fig. 7.

The steady state equilibrium analysis of the motion of a wheel set traveling on a track with a constant curvature is based, in this paper, on the following assumptions:
- The wheel set center of gravity moves with a constant prescribed forward velocity along the tangent to the track centerline.
- The wheel set has one point of contact on the wheel that travels on the inner rail (left) and two points of contact on the wheel that travels on the outer rail (right).

- The wheel set has unknown constant roll and yaw angles. That is, while the roll and yaw angles are to be determined, their derivatives with respect to time are assumed to be zero.
- The wheel set angular velocity about its axis is constant.
- Friction forces (creep forces) are assumed to be functions of the relative velocities of the points of contact, normal contact forces, local geometry of wheel and rail at the contact points and material elastic properties (Kalker's nonlinear creep theory [13]).

Note that because of these assumptions, all the accelerations are equal to zero with respect to the track coordinate system, and the resulting dynamic problem, which is not an inverse dynamic problem, leads to a set of algebraic equations that can be solved for the unknown coordinates and forces as discussed in the following sections.
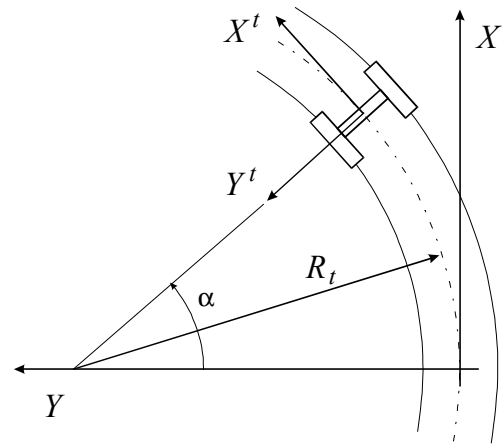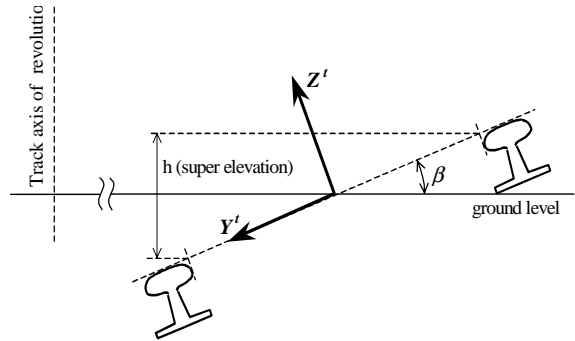

Figure 6. Track coordinate system.

Figure 7. Orientation of the track coordinate in case of superelevation.

3.1. Wheel Set Position Analysis

At any contact point P between the wheel set and the rail, the position vector of the contact point can be written in terms of the following vector of surface parameters:

$$\mathbf{s}_P = \begin{bmatrix} s_{1\,P}^r & s_{2\,P}^r & s_{1\,P}^w & s_{2\,P}^w \end{bmatrix}^T, \quad (6)$$

and the following five nonlinear constraint equations must be fulfilled [16]:

$$\mathbf{C}_P = \mathbf{0}, \quad (7)$$

where

$$\begin{bmatrix} C_{P1} & C_{P2} & C_{P3} \end{bmatrix}^T = \mathbf{r}_P^w - \mathbf{r}_P^r, \Bigg\}$$
$$C_{P4} = \mathbf{n}_P^{r^T} \mathbf{t}_{lP}^w, \quad C_{P5} = \mathbf{n}_P^{r^T} \mathbf{t}_{tP}^w, \Bigg\} \quad (8)$$

where $\mathbf{n}_P^r$ is the normal to the rail at the contact point, $\mathbf{t}_{lP}^w$ is the longitudinal (in the $s_{2\,P}^w$ direction) tangent to the wheel at the contact point, and $\mathbf{t}_{tP}^w$ is the transverse (in the $s_{1\,P}^w$ direction) tangent to the wheel at the contact point. The first three constraints in Eq. 8 are the *contact point constrains* that guarantee that a point on the surface of the wheel (point of contact on the wheel) has the same global position as a point on the surface of the rail (point of contact on the rail). The last two constraints in Eq. 8 are the *orientation constrains*, that guarantee that the tangent plane at the contact point on the wheel is parallel to the tangent plane at the contact point on the rail. In what follows, subscript L refers to the contact point on the tread of left wheel, subscript R refers to the contact point on the tread of the right wheel, and subscript F refers to the contact point on the flange of the right wheel. The generalized and non-generalized coordinates of the wheel set with three points of contact are:

$$\mathbf{q} = \begin{bmatrix} \mathbf{R}^{w^T} & \boldsymbol{\theta}^{w^T} & \mathbf{s}_L^T & \mathbf{s}_R^T & \mathbf{s}_F^T \end{bmatrix}^T, \quad (9)$$

and the following system of 15 contact constraint equations must be satisfied:

$$\mathbf{C} = \begin{bmatrix} \mathbf{C}_L^T & \mathbf{C}_R^T & \mathbf{C}_F^T \end{bmatrix}^T = \mathbf{0}. \quad (10)$$

Therefore, there are 18 coordinates and 15 constraint equations, leading to a three-degree of freedom wheel set system. Out of the three degrees of freedom, two degrees of freedom do not affect the solution of the problem discussed in this section. Recall that an assumption is made that all the wheel set accelerations are equal to zero with respect to the track coordinate system $X^t Y^t Z^t$ and all forces and moments that act on the wheel set are constant in this track frame. The relative position of the wheel set with respect to the rails is independent of the longitudinal position along the track. Hence, in what follows, the position and orientation of the wheel set is analyzed at $X^w = 0$. In this position, the origin of the global coordinate system and the origin of the track coordinate system coincide. Since the wheel set is a solid of revolution, the rotation of the wheel about its axis does not affect the position analysis. In other words, if the surface parameters $s_{2\,L}^w, s_{2\,R}^w, s_{2\,F}^w$ (angular orientation of the contact points on the wheel set) belong to a solution $\mathbf{q}$ of the system of constraints of Eq. 10, then the set $s_{2\,L}^w + \delta, \; s_{2\,R}^w + \delta, \; s_{2\,F}^w + \delta$, where δ is an arbitrary angle, also belong to a solution $\mathbf{q}^*$ that only differs from $\mathbf{q}$ by a rotation δ of the wheel set about its axis. For this reason, in the position analysis performed in this study and without any loss of generality, the angular parameter of the left wheel $s_{2\,L}^w$ is assumed to be specified, thereby eliminating the freedom of the wheel rotation about its axis. By

specifying X^w and $s_{2\,L}^w$ the number of degrees of freedom of the wheel set reduces to one.

In principle, the system of nonlinear constraints of Eq. 10 can be solved using as independent coordinate the yaw angle ϕ of the wheel set which will be determined in later sections using the force balance algebraic equations. Nonetheless, the algebraic kinematic equations obtained in this section can be solved for a wide range of values of the yaw angle, which has been varied using small increments, as shown in Fig. 8. The small yaw angle can be defined using the x component of the $\mathbf{j}^w$ unit vector of the wheel set (aligned with the wheel axle) as shown in Fig. 8. In the numerical study presented in this section, the wheels are assumed to be profiled with approximate conicity of 1/40, while the rail profile is assumed to be of the AREA type. Geometrical properties of the wheel set and rails are provided in Fig. 9. It is important to point out that the value of the yaw angle ϕ is restricted by a certain wheel set configuration in which a second point of contact also occurs at the left wheel. In this position, the wheel set has four points of contact with the rails. Notice that in this extreme position the wheel set is in an anti-symmetric position with respect to the normal to the track (Y^t). Therefore, the wheel set has to be centered, this is the case in which $R_y^w = 0$.

When the yaw angle is zero, the first and second points of contact on the right wheel are contained in one plane perpendicular to the rail, that is, the two points of contact have the same s_1^r and s_2^w parameters. However, when the yaw angle increases, the difference between these parameters that correspond to the two points of contact increases. This is known as the lead (negative yaw) and lag (positive yaw) contact. Elkins and Weinstock [2] provide an expression to evaluate these differences (this expression was obtained by Bödecker [14]), as follows:

$$\Delta s_1^r = r_1 \phi \tan \delta, \quad \Delta s_2^w = \arctan(\phi \tan \delta) \quad (11)$$

where r_1 is the radius of the wheel at the first point of contact, δ is the angle of attack at the flange contact, and ϕ is the yaw angle. Figure 10 shows the results of the solution of Eq. 10 compared with the expressions given by Eq. 11. An excellent agreement can be observed. Notice that for small values of the yaw angle, the increase in the surface parameters is approximately linear.
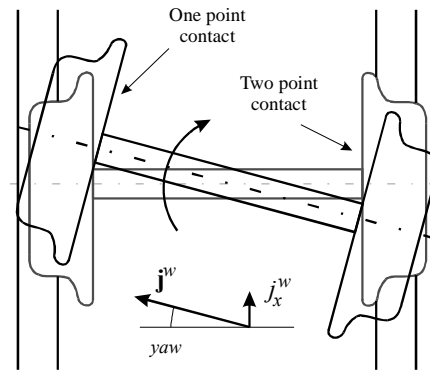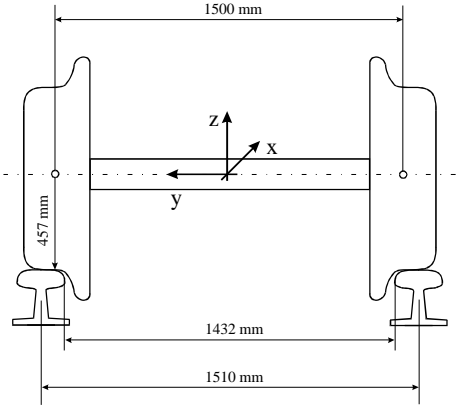

Figure 8. Yaw rotation.

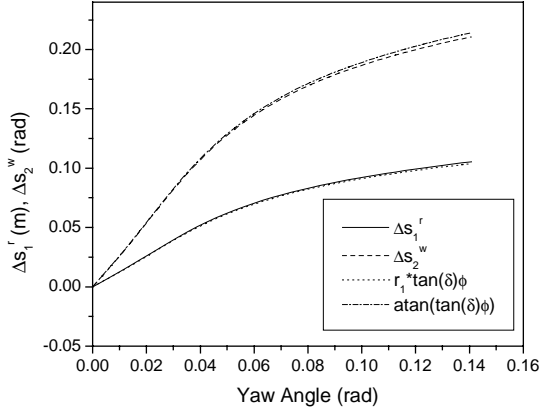Figure 9. Geometry of wheel set and rails.

Figure 10. Relative position of second point of contact on the right wheel.

3.2. Wheel Set Velocity Analysis

As previously pointed out, the wheel set center of gravity is assumed to move with constant forward velocity V along the track. The wheel set lateral motion is not constrained, however, the existence of three points of contact and the fact that the yaw remains constant prevent any lateral velocity of the wheel set. Therefore, the wheel set translational velocity is given by

$$\dot{\mathbf{R}}^w = \mathbf{A}^t \begin{bmatrix} V & 0 & 0 \end{bmatrix}^T, \qquad (12)$$

where $\mathbf{A}^t$ is the rotation matrix that defines the orientation of the track coordinate system with respect to the global coordinate system.

A systematic procedure for the velocity analysis is to evaluate the derivatives of the constraints of Eq. 10. Once the position analysis is completed, differentiation of the constraints of Eq. 10 leads to a system of algebraic equations that is linear in the velocities. While as previously explained, the parameter $s_{2\,L}^w$ has no effect on the solution of the position equations, the angular velocity $\dot{s}_{2\,L}^w$ of the wheel set about its own axis is not zero and its value will be determined in a later section using the algebraic force balance equations. Based on the assumptions made in *steady state equilibrium analysis*, the time derivatives of the surface parameters are directly determined using the following equations:

$$\dot{s}_{1\,P}^r = \frac{R_P}{R_t} V, \quad \dot{s}_{2\,P}^r = 0, \quad \dot{s}_{2\,P}^w = 0, \qquad (13)$$

$$\dot{s}_{1\,P}^w = 0 = \Omega, \qquad P = L, R, F$$

where R_P is the distance in the plane XY from the contact point to the center of curvature of the track, R_t is the radius of curvature of the track , and Ω is the magnitude of the angular velocity of the wheel set about its axis. If the angular velocity of the wheel set Ω is known, Eqs. 12 and 13 can be used to define $\dot{\mathbf{R}}^w, \dot{\mathbf{s}}_L, \dot{\mathbf{s}}_R$ and $\dot{\mathbf{s}}_F$.

The absolute angular velocity of the wheel set used in the model discussed in this investigation can be divided into two components. One is due to the rotation of the wheel set about the Z axis, and the other is due to the rotation of the wheel set about its own axis. Therefore, the absolute angular velocity can be written as:

$$\boldsymbol{\omega}^w = \begin{bmatrix} 0 & 0 & \dfrac{V}{R_t} \end{bmatrix}^T + \Omega \mathbf{j}^w \qquad (14)$$

where Ω can assume an arbitrary value that will be determined using the procedure described later in this paper.

It can be shown that the velocities defined by Eqs. 12-14 satisfy the constraints of Eq. 8 at the velocity level. The constraints at the velocity level can be used to show that the absolute velocities of the three contact points lie in planes tangent to the surfaces of the wheel and the rail at the contact points, that is, the component of the velocity along the normal to the contact surface is always equal to zero. This result is easily understood from the derivative of the first three constraints of Eqs. 8, which leads to

$$\dot{\mathbf{r}}_P^w - \dot{\mathbf{r}}_P^r = \mathbf{0} \qquad (15)$$

which can be written as

$$\mathbf{v}_P^w = \dot{\mathbf{R}}^w + \dot{\mathbf{A}}^w \overline{\mathbf{u}}^w = \dot{s}_1^r \mathbf{t}_l^r + \dot{s}_2^r \mathbf{t}_t^r - \dot{s}_2^w \mathbf{t}_l^w - \dot{s}_1^w \mathbf{t}_t^w \qquad (16)$$

where $\mathbf{v}_P^w$ is the apparent velocity of the contact point on the wheel, and $\mathbf{t}_l^r$, $\mathbf{t}_t^r$, $\mathbf{t}_l^w$, and $\mathbf{t}_t^w$ are not assumed to be unit vectors. Note that the second and fourth terms on the right hand side of Eq. 16 are identically zero in this particular problem. If the wheel set does not rotate about its own axis, the wheel set has to follow a circular path along the center of curvature of the track in order to maintain the three points of contact. Therefore, the first component of the angular velocity given in Eq.14 is necessary in order to satisfy Eq. 16. Furthermore, the angular velocity of the wheel about its axis leads to non-zero velocity components for the points on the wheel surface in the direction of the vector $\mathbf{t}_l^w$ only. Therefore, these velocities also satisfy Eq. 16.

Note that in the position analysis discussed in the preceding section and the velocity analysis discussed in this section, the following sequence was used:

- The position equations of the wheel set were expressed in terms of one degree of freedom. The yaw angle can be conveniently selected as the independent parameter. Once the value of the yaw angle is determined as described in Section 3.3, the position of the three contact points in the wheel set coordinate system, the vertical and transverse displacements, and the orientation of the wheel set (except for the rotation of the wheel set about its axis) can be determined.
- Once the position coordinates of the wheel set are determined, the velocities of the wheel set can be determined as functions of the wheel set angular velocity Ω about its axis. Once the angular velocity Ω is determined as described in Section 3.3 and using the results of the position analysis (knowledge of the rotation of the wheel set about its axis is not required), the reference velocities of the wheel set as well as the time derivatives of the surface parameters and the velocity of the contact points can be determined.

It is important to point out at this point that the selected independent kinematic parameters, the yaw angle ϕ and the wheel set angular velocity Ω, are assumed to be constant but they are not constrained. Therefore, the problem discussed in this section is not an inverse dynamics problem. The dynamic force balance, discussed later, will be used to determine the angular velocity and the yaw angle of the wheel set when it negotiates curved tracks under the assumed conditions.

3.3. Wheel Set Forces

Since the dynamic force balance of a rigid body provides six independent algebraic equations, six independent unknowns can be determined. The constraint contact forces and the force associated with the constraint of the wheel set prescribed forward velocity are included in these unknowns. As discussed in previous publications [15], there is only one independent constraint force associated with the five constraints of each contact. Therefore, four unknown scalar forces determine the contact constraints and the constraint on the wheel set forward velocity. The dynamic force balance provides two additional equations that are used to obtain the yaw angle ϕ and the angular velocity Ω. In the following, the forces and moments that act on the system are expressed as a function of the system coordinates and velocities.

Creep Forces and Moments Among the unknowns of the wheel set problem considered in this investigation are the three scalar values of the normal contact force at the points of contact. The vector of normal contact forces is given by

$$\mathbf{F}_n = \begin{bmatrix} F_{nL} & F_{nR} & F_{nF} \end{bmatrix}^T \qquad (17)$$

The forces in the planes tangent to the contact surfaces and the spin moments that have the direction of the normal to the surfaces can be determined using Kalker's nonlinear creep theory [13]. These forces and moments are functions of the normal contact forces, local surface geometry properties (semi axis of the contact ellipses, principal radius of curvature), material properties, relative velocity at the contact points (creepages), and coefficient of friction. In order to evaluate the local surface geometry properties that depend on the surface

parameters, the step of the position analysis must be considered; and in order to evaluate the creepages, the velocity components must be determined. That is, all the position variables must be expressed in terms of the yaw angle ϕ, and all the velocities must be expressed in terms of ϕ and the angular velocity Ω. The creep forces and moments are obtained as:

$$\left. \begin{array}{l} \mathbf{F}_{cP} = \mathbf{A}^P \begin{bmatrix} F_{xP} & F_{yP} & 0 \end{bmatrix}^T , \\[2mm] \mathbf{M}_{cP} = \mathbf{A}^P \begin{bmatrix} 0 & 0 & M_{cP} \end{bmatrix}^T , \quad P = L, R, F \end{array} \right\} \qquad (18)$$

where F_{xP} and F_{yP} are the tangential creep force components, M_{cP} is the spin moment, and $\mathbf{A}^P$ is the rotation matrix that defines the orientation of the surface coordinate system at the contact point with respect to the global coordinate system. The X-axis of the surface coordinate system is the tangent to the rail in the longitudinal direction, the Y-axis is the tangent to the rail in the lateral direction, and as Z-axis is in the direction of the normal to the rail surface at the contact point.

Inertia Forces and Moments The inertia forces due to the centrifugal force are simply given by

$$\mathbf{F}_i = \left(-\frac{mV^2}{R_t} \right) \mathbf{A}^t \begin{bmatrix} 0 & -\cos\beta & \sin\beta \end{bmatrix}^T \qquad (19)$$

where $\mathbf{A}^t$ is the transformation matrix that defines the orientation of the track coordinate system as previously defined, and β is the angle of superelevation, shown in Fig. 7. The inertia moments can be evaluated as the derivative of the angular momentum. The angular velocity of the wheel set defined by Eq. 14 is constant in the track coordinate system (because the wheel set coordinate system has a fixed orientation with respect to the track coordinate system). Therefore, the angular momentum vector, which is also constant in the track coordinate system, is given by

$$\mathbf{L}_w = \mathbf{A}^t \mathbf{L}_w^t = \mathbf{A}^t \left(\mathbf{A}^{tw} \mathbf{J} \mathbf{A}^{tw^T} \mathbf{A}^{t^T} \boldsymbol{\omega}^w \right) = \mathbf{A}^t \left(\mathbf{A}^{tw} \mathbf{J} \mathbf{A}^{w^T} \boldsymbol{\omega}^w \right) \qquad (20)$$

where $\mathbf{L}_w$ is the angular momentum defined in the global coordinate system, $\mathbf{L}_w^t$ is the angular momentum defined in the track coordinate system, $\mathbf{A}^{tw} = \mathbf{A}^{t^T} \mathbf{A}^w$ is the rotation matrix from the wheel set to the track coordinate systems (assumed constant), $\mathbf{J}$ is the inertia tensor in the wheel set coordinate system (assumed diagonal and constant), and $\boldsymbol{\omega}^w$ is the angular velocity vector of the wheel set given by Eq. 14. All terms given between brackets in Eq. 20 are constant. Therefore, the inertia moments are obtained as

$$\mathbf{M}_i = -\frac{d}{dt}(\mathbf{L}_w) = -\dot{\mathbf{A}}^t \mathbf{A}^{tw} \mathbf{J} \mathbf{A}^{w^T} \boldsymbol{\omega}^w \qquad (21)$$

The time derivative $\dot{\mathbf{A}}^t$ is a linear function of the derivative of the angle α shown in Fig. 6. By the virtue of the forward velocity constraint, one has

$$\alpha = \frac{V}{R_t} t, \quad \dot{\alpha} = \frac{V}{R_t} \qquad (22)$$

Driving Constraint and Gravity Force The forward velocity constraint has an associated driving force F_f that balances all other longitudinal forces, leading to a zero longitudinal acceleration. This force can be determined and defined in the track coordinate system using the following transformation:

$$\mathbf{F}_f = \mathbf{A}^t \begin{bmatrix} F_f & 0 & 0 \end{bmatrix}^T \qquad (23)$$

The gravity force is given by the vector

$$\mathbf{W} = \begin{bmatrix} 0 & 0 & -mg \end{bmatrix}^T \qquad (24)$$

Force Balance The force and moment balances are defined by the following two equations:

$$\sum_{P=L,R,F} \left(F_{nP} \mathbf{n}_P + \mathbf{F}_{cP} \right) + \mathbf{F}_i + \mathbf{F}_f + \mathbf{W} = \mathbf{0} \qquad (25)$$

$$\sum_{P=L,R,F} \left(\left(\mathbf{r}_P^w - \mathbf{R}^w \right) \times \left(F_{nP} \mathbf{n}_P + \mathbf{F}_{cP} \right) + \mathbf{M}_{cP} \right) + \mathbf{M}_i = \mathbf{0} \qquad (26)$$

The unknowns in these six nonlinear algebraic equations are the yaw angle ϕ, the angular velocity Ω, the driving constraint force F_f, and the three normal contact forces F_{nL}, F_{nR}, and F_{nF}.

To this end, the solution of Eqs. 10 together with the dynamic Eqs. 25 and 26. provides the position and orientation of the wheel set as well as the forces involved in the steady state curving behavior. Instead of eliminating some variables, as another alternative, a large system of nonlinear equations can be considered. The unknowns in this system of equations are $\mathbf{R}^w, \mathbf{\theta}^w, \mathbf{s}_L, \mathbf{s}_R, \mathbf{s}_F, \Omega, \mathbf{F}_n, F_f$. These unknowns can be determined by solving the following system of nonlinear algebraic equations:

$$\left. \begin{array}{l} \mathbf{C}_L = \mathbf{0}, \mathbf{C}_R = \mathbf{0}, \mathbf{C}_F = \mathbf{0}, \\ X^w = 0, s_{2I}^w = 0, \\ \sum_j \mathbf{F}_j = \mathbf{0}, \sum_j \mathbf{M}_j = \mathbf{0} \end{array} \right\} \qquad (27)$$

where $\mathbf{F}_j$ and $\mathbf{M}_j$ represent, respectively, all forces and moments acting on the system. The dynamic equilibrium problem has 23 unknowns and 23 non-linear algebraic equations. However, as an alternative, the dimension of the problem can be reduced in order to efficiently obtain the numerical solution. As previously demonstrated, the position analysis can practically be completed using one degree of freedom, the yaw angle ϕ. It is important to point out that among the results that can be obtained from the solution of Eqs. 27 are position coordinates, which are not necessarily unique. Furthermore, the equilibrium positions found could be stable or

unstable in response to disturbances. However, as it is known unsuspended wheel sets have stability problems that have been the subject of investigations in the literature.

4. MULTIBODY DYNAMIC FORMULATIONS

In multibody dynamics there are two common methods to analyze the contact between rigid bodies. These are the elastic method and the constraint method. These two methods are briefly described in this section.

Elastic Method In the elastic method [11], the rigid bodies are allowed to interpenetrate in the neighborhood of the contact point. The contact points, where the contact forces are applied, are found through a search process. The resulting contact force can be evaluated as a function of the indentation of the bodies (elastic component) and the velocity of indentation (damping component). In the multibody dynamic formulation used in this investigation, the following expression for the contact force is used:

$$F = F_h + F_d = -K_h \delta^{3/2} - C \dot{\delta} |\delta| \qquad (28)$$

where δ is the indentation, F_h is the Herzian (elastic) contact force, F_d is the damping force, K_h is the Hertzian constant that depends on the surface curvatures and the elastic properties, and C is a damping constant. Creepage forces are included using Kalker's non-linear creep theory [13]. Creepage forces are functions of the relative velocity of the points of contact, normal contact force, the local geometry of wheel and rail at the contact points and material elastic properties

When using the elastic method, the augmented form of the equations of motion can be written as follows [16]:

$$\begin{bmatrix} \mathbf{M} & \mathbf{C}_q^T \\ \mathbf{C}_q & \mathbf{0} \end{bmatrix} \begin{bmatrix} \ddot{\mathbf{q}} \\ \mathbf{\lambda} \end{bmatrix} = \begin{bmatrix} \mathbf{Q} \\ \mathbf{Q}_d \end{bmatrix} \qquad (29)$$

where $\mathbf{M}$ is the system mass matrix, $\mathbf{C}_q$ is the Jacobian matrix of the kinematic constraints, $\mathbf{q}$ is the vector of the system generalized coordinates, $\mathbf{\lambda}$ is the vector of Lagrange multipliers, $\mathbf{Q}$ is a vector that includes external, applied contact, creep, and centrifugal and Coriolis forces, and $\mathbf{Q}_d$ is the vector that results from the differentiation of the constraint equations twice with respect to time, that is

$$\mathbf{C}_q \ddot{\mathbf{q}} = \mathbf{Q}_d \qquad (30)$$

The vector of kinematic constraint equations $\mathbf{C}$ ($\mathbf{q}$, t) = $\mathbf{0}$ describes mechanical joints as well as specified motion trajectories that include driving constraints. Such driving constraints include the specified forward velocity of the wheel sets.

In this investigation, the elastic force model is not used in the case of the inverse dynamic analysis. In the inverse dynamic analysis, all contacts including the flange contact are modeled using the constraint method. However, the elastic method is used in this investigation in the case of the forward dynamics, allowing for wheel/rail separation.

Constraint Method In the constraint method [15,16], the contact between the bodies is described using non-linear kinematic constraint equations that are expressed in terms of

Copyright © 2003 by ASME

the wheel set coordinates as well as the surface parameters at the contact points. Five kinematic constraint equations, as defined in Eq. 8, are used to describe the general contact between two rigid bodies [15,16]. Three of these five constraints (C_{P1}, C_{P2} and C_{P3}), called contact point constraints, impose the conditions that two points on the two bodies coincide during the dynamic motion while avoiding penetration and separation. The remaining two constraints (C_{P4} and C_{P5}), called orientation constraints, impose the condition that the normals to the surfaces at the contact point are parallel. Since four new surface parameters are introduced, the preceding independent five contact constraint equations can be used to eliminate only one generalized degree of freedom. Therefore, in this formulation, a wheel has five degrees of freedom with respect to the rail in the case of a single contact point.

In general, the kinematic constraint equations, including the contact constraints, imposed on the motion of a multibody system can be expressed in the following vector form:

$$\mathbf{C}(\mathbf{q}, \mathbf{s}, t) = \mathbf{0} \tag{31}$$

where $\mathbf{C}$ is the vector of constraint functions, $\mathbf{q}$ is the vector of the system generalized coordinates, $\mathbf{s}$ is the vector of the system non-generalized surface parameters, and t is time. Differentiating the preceding equation twice with respect to time and combining the resulting acceleration equations with the Lagrangian form of the equations of motion expressed in terms of Lagrange multipliers, one obtains the following augmented form of the equations of motion of the multibody system subject to contact constraints [15,16]:

$$\begin{bmatrix} \mathbf{M} & \mathbf{0} & \mathbf{C}_\mathbf{q}^T \\ \mathbf{0} & \mathbf{0} & \mathbf{C}_\mathbf{s}^T \\ \mathbf{C}_\mathbf{q} & \mathbf{C}_\mathbf{s} & \mathbf{0} \end{bmatrix} \begin{bmatrix} \ddot{\mathbf{q}} \\ \ddot{\mathbf{s}} \\ \lambda \end{bmatrix} = \begin{bmatrix} \mathbf{Q} \\ \mathbf{0} \\ \mathbf{Q}_d \end{bmatrix} \tag{32}$$

where $\mathbf{M}$ is the system mass matrix, λ is the vector of Lagrange multipliers, $\mathbf{Q}$ is a vector that includes external, creep, and centrifugal and Coriolis forces, and $\mathbf{Q}_d$ is a quadratic velocity vector that results from differentiating the kinematic constraints twice with respect to time [16]. Note that the preceding augmented form of the equations of motion is expressed in terms of the generalized coordinates $\mathbf{q}$ as well as the non-generalized surface parameters $\mathbf{s}$ and their time derivatives.

Two-Point Contact   In this section, two conceptually different methods, the elastic and the constraint methods, are discussed for the analysis of the wheel/rail interaction [11] These two methods can be used as the basis for three different procedures to study the two-point contact problem. In the first procedure, the elastic force model that allows six degrees of freedom for the wheel with respect to the rail is used. This method also allows for the wheel lift. As mentioned in this section, a search is made in order to determine the contact points. Therefore, the elastic force model can be directly used to study the two-point contact by limiting the number of contact points for each wheel to two. The forces at the two contact points can be calculated as previously described in this paper.

The second procedure that can be used in the analysis of the two-point contact is to model all the contacts using the constraint method. This procedure, that employs a multibody system formulation, allows using the same assumptions used in the simple model described in the preceding section. This method will be used in the inverse dynamic multibody solution presented in the second part of this paper. Note that in the multibody simulation algorithm, no variables are eliminated and Lagrange multipliers are used to determine the normal contact forces, which is not the case when the formulation presented in the preceding sections is used.

A third procedure that can be used in the analysis of the two-point contact is a hybrid method. In this hybrid method, which allows only five degrees of freedom for the wheel with respect to the rail, the first point of contact is predicted using the contact constraint approach, while the second point of contact is determined using the elastic approach. The second point of contact is obtained by numerically searching for a point of contact different from the first point that is determined using the kinematic contact constraints. In the hybrid method, the normal force at the first point of contact is determined using Lagrange multipliers, while the normal force at the second point of contact is determined using the elastic approach described in this paper [11].

5. SOLUTION OF THE STEADY STATE EQUILIBRIUM ANALYSIS

The curving behavior of a wheel set is analyzed in this section using the specialized method of the steady state equilibrium analysis. The wheel set has the same geometric properties as the model used in the first part of this paper. The wheel set mass is assumed to be 1568 Kg and the mass moments of inertia are assumed to be $I_{yy} = 168$ Kg·m^2, $I_{xx} = I_{zz} = 656$ Kg·m^2. The coefficient of friction between the wheel and the rail is assumed to be 0.5. Both the wheel set and the rail are assumed to be made of steel with Young's modulus $E = 2.1 \times 10^{11}$ N/m^2 and Poisson's ratio $v = 0.3$.

Effect of the Forward Velocity   Three sets of solutions have been obtained using constant track curvatures of 3, 5 and 7 deg (100'-chord definition) and zero superelevation. The system of Eqs. 27 has been solved for a wide range of the forward velocities. The yaw angle obtained as one of the solutions of this system of equations is shown in Fig. 11 as function of the forward velocity. It can be observed from the results presented in this figure that the yaw angle increases as the forward velocity increases. The rate of change of the yaw angle increases as the curvature increases. For low forward velocities, the yaw angle is negative. Note that the yaw angle becomes positive at forward velocities of 36.2 m/s and 42.5 m/s and 46.8 m/s, in the case of track curvatures 7 deg, 5 deg and 3 deg, respectively.

Figure 12 shows the normal contact forces at the treads. The forces on the right wheel increase and the forces on the left wheel decreases as the forward velocity increases. The rate of change of these forces increases as the track curvature increases. Figure 13 shows the normal force at the flange contact as a function of the forward velocity. The force increases as the forward velocity increases, and the rate of change increases as the curvature increases.
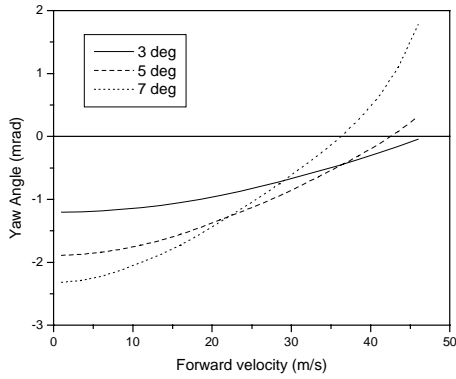
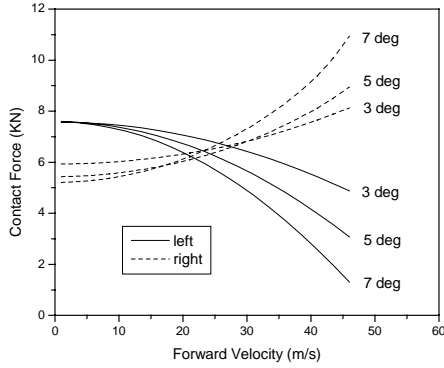Figure 11. Yaw angle as function of the forward velocity.

Figure 12. Normal contact forces at the treads as functions of the forward velocity.
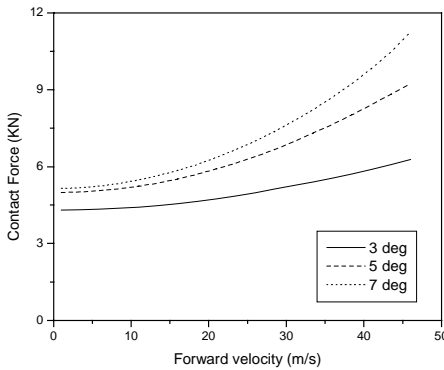

Figure 13. Normal contact forces at the right flange as functions of the forward velocity.

The change of yaw angle from negative at low forward velocity to positive at high forward velocity is now analyzed in detail. Figure 14 shows the change in direction of the sliding velocity of the contact points for negative and positive yaw angles. In this analysis, the absolute velocity of the contact point is $\mathbf{v}_s = \dot{\mathbf{R}}^w + \boldsymbol{\omega}^w \times \mathbf{u}$, where $\dot{\mathbf{R}}^w$ is the absolute velocity vector of the wheel set center of mass, $\boldsymbol{\omega}^w$ is the absolute angular velocity vector of the wheel set, and $\mathbf{u}$ is the location of the contact point with respect to the wheel set center of mass. In this case, $v_s = \left| \mathbf{v}_s \right|$, $v_f = \left| \dot{\mathbf{R}}^w \right|$, and $v_r = \left| \boldsymbol{\omega}^w \times \mathbf{u} \right|$.

Since the creep forces have opposite direction to the sliding velocity of the contact points, a negative yaw creates negative lateral creep forces and a positive yaw creates positive lateral creep forces.

(a) Low velocity   (b) High velocity
(negative yaw)   (positive yaw)
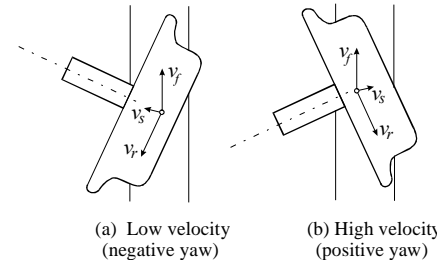
Figure 14. Sliding velocity of tread contact points.

The change in the sense of the yaw angle at low and high velocities can be explained considering the balance of the moments about the X axis of the track coordinate system.
Low Velocity. At low velocity the centrifugal force and gyroscopic moment are small. Each of the vertical contact forces on the left and right wheels (including flange and tread vertical contact forces) are approximately half the weight of the wheel set. In the case of zero yaw angle, the sliding component of the tread contact points in the lateral direction vanishes ($F_{xL} = F_{xR} = 0$ and as a consequence the moments in Fig. 15 are identically zero). In this case, there is clearly an unbalanced positive roll moment. Therefore, the case of zero yaw angle should not occur at low velocities, instead a negative yaw angle occurs in order to create the necessary forces (F_{xL} and F_{xR}) that produce the moments that counterbalance the roll moment (see Figure 15) and maintains equilibrium.
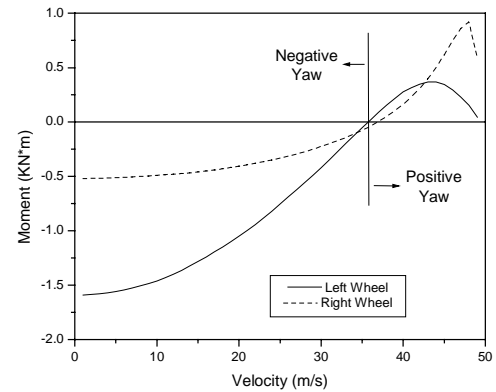

Figure 15. Roll moments of tread lateral forces.

High Velocity. At high velocity the centrifugal force and gyroscopic moment are large. The vertical contact force on the right wheel is larger that the vertical contact force on the left wheel. In this case, if the yaw is zero (tread contact points do not slide in the lateral direction) there is an unbalance negative roll moment. Therefore, the wheel set must have a positive yaw angle that creates the necessary forces (F_{xL} and F_{xR}) that produce the moments that counterbalance the roll moment (see Fig. 15) in order to maintain equilibrium.
Effect of the Track Curvature Assuming forward velocities of 10, 15 and 20 m/s another set of results was

10

obtained for a wide range of curvatures. Figure 16 shows the yaw angle as a function of the track curvature. As can be observed, the absolute value of the yaw angle decreases as the forward velocity increases. The three curves show the same behavior, initially the absolute value of the yaw increases when increasing the curvature up to a certain maximum value (0.0024 rad at 15 m/s, 0.0018 rad at 9m/s and 0.00145 rad at 6.5 m/s for forward velocities 10, 15 and 20 m/s, respectively). After reaching the maximum value, the absolute value of the yaw angle starts to decrease as the curvature increases.

Figure 17 shows the normal contact forces at the treads as function of the curvature of the track. The forces on the left wheel decrease with a constant slope as the curvature increases, and the rate of change increases as the forward velocity increases. Forces on the right wheel show an interesting behavior: initially the force decreases as the curvature increases up to a value of approximately 3.5 deg. After that point, there is a change in the slope of the curves, and the force decreases for forward velocity of 10 and increases for 15 and 20 m/s. All forces seem to converge to 7.7 KN (half weight of the wheel set) for an extrapolated curvature of 1 deg, which corresponds to a configuration with two points of contact (no flange contact). Figure 18 shows the normal force at the flange contact versus the track curvature. The force increases at a high rate up to 3.5 deg, at that point the slope of the curves decreases, and the force increases at a constant rate. Note that the rate of change increases as the forward velocity increases. The forces seem to converge to zero for an extrapolated curvature of 1 deg, which corresponds to a configuration with two points of contact (no flange contact).
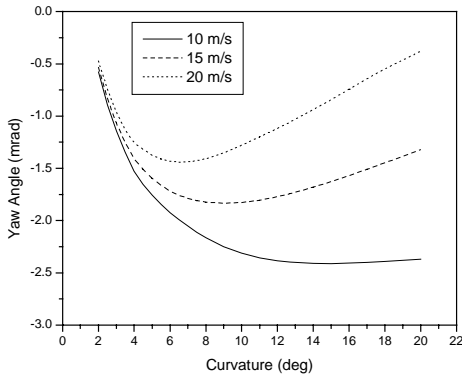

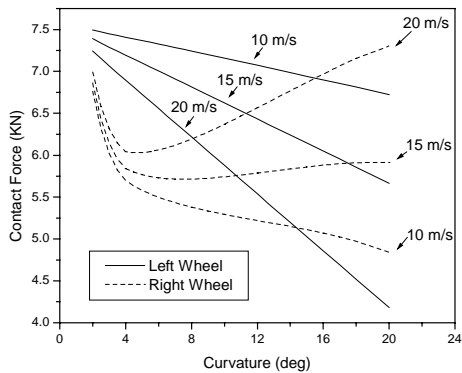Figure 16. Yaw angle as function of the track curvature.

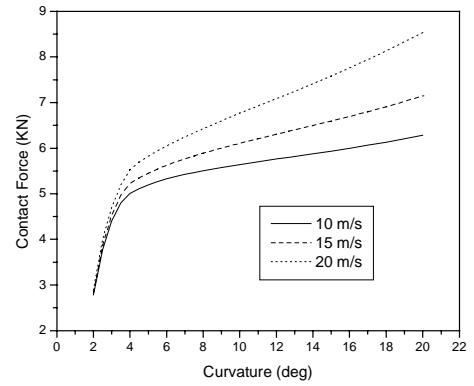Figure 17. Normal contact forces as functions of the track curvature.

Figure 18. Flange force as function of the track curvature.

Effect of Superelevation A third set of results was obtained for different superelevations with forward velocities of 10, 15 and 20 m/s and track curvature of 5 deg. The superelevation is expressed in terms of percentage of *balanced superelevation*, which is evaluated by equating the centrifugal force with the transverse component of the weight, as follows:

$$\tan(\alpha_{balanced}) = \frac{V^2}{gR_t} \tag{33}$$

$$h_{balanced} = G\sin(\alpha_{balanced}) \tag{34}$$

where $\alpha_{balanced}$ is the angle of balanced superelevation, V is the forward velocity, g is the gravity constant, R_t is the radius of curvature of the track, $h_{balanced}$ is the height of balanced superelevation, and G is the gage distance. For the model data used, forward velocities of 10, 15 and 20 m/s and curvature of 5 degrees, the balanced superelevations are 42, 94 and 163 mm, respectively.

Figure 19 shows that the absolute value of the yaw angle increases as the superelevation increases. For low superelevation, the change rate is constant, and it is larger for higher velocities. Figure 20 shows the normal contact forces at the treads. The force on the left tread increases as the superelevation increases, whereas the force on the right tread decreases. The slope of the curves increases as the velocity increases. Figures 21 shows the normal contact force at the flange. The flange forces decreases as the superelevation increase and the rate of change increases as the forward velocity increases.
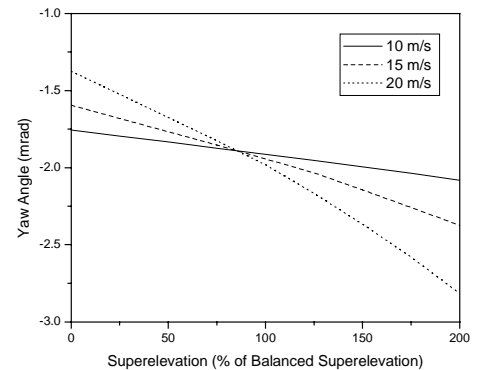

Figure 19. Yaw angle as function of the superelevation.
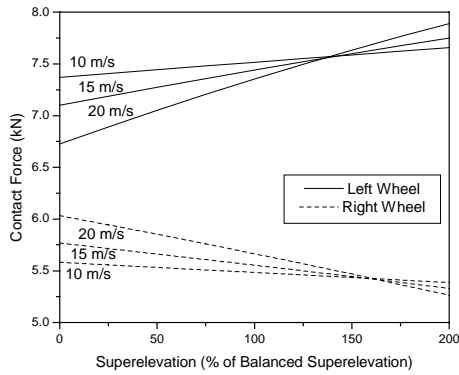
11   Copyright © 2003 by ASME

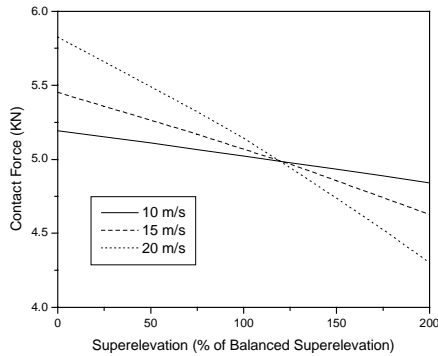Figure 20. Normal contact forces at the treads as functions of the superelevation.

Figure 21. Normal contact forces at the flange as functions of the superelevation.

6. COMPARISON WITH MULTIBODY FORMULATIONS

In this section, the results of the specialized steady state wheel set formulation are compared with the results of the inverse dynamics multibody solution and the results of the forward dynamic solution.

A wheel set moving on a 5 deg track has been analyzed with forward velocities of 10, 20, 30 and 40 m/s. Figure 22 shows the normal contact forces obtained using the inverse dynamics analysis for different forward velocities. The results are compared with the contact forces obtained in the specialized steady state formulation. Excellent agreement has been found without noticeable discrepancies.
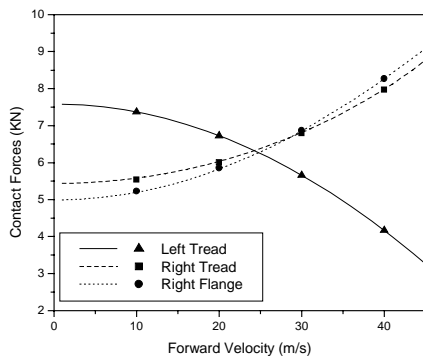

Figure 22. Normal contact forces in inverse dynamics analysis

In the case of the forward dynamics, a wheel set with the same properties used in the specialized steady state dynamic equilibrium analysis is assumed to travel on a track that consists of three segments. The first is a tangent segment with zero superelevation, the second is a spiral-entry segment (linear variation of curvature and superelevation along the longitudinal coordinate), and the third is a constant curvature segment with curvature and superelevation that will be specified later. The first two segments are used to make the entry of the wheel set into the curved track as smooth as possible, thereby avoiding impulsive flange impacts. When the wheel set enters the spiral segment, the flange of the right wheel contacts the gage face of the rail. A short distance after entering the constant curvature segment the wheel set shows a steady state behavior (position with respect to the track coordinate system is constant). The dynamic forces at the three contact points are projected onto the track coordinate system and averaged over a time window. As an example of the results of the dynamics simulation, Fig. 23 shows the contact forces on the tread of the left and right wheels and the flange of the right wheel during the motion of the wheel set. Here the results are obtained using the elastic approach, forward velocity of 5 m/s and, in the constant curvature segment, the track has 5 deg with balanced superelevation. It can be observed that the contact forces have high frequency oscillations that are typical when the elastic approach is used, but the average values are approximately constant during curve negotiation. This is due to the large stiffness associated with the elastic contacts.
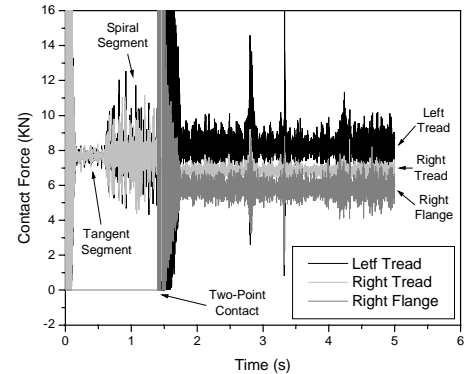

Figure 23. Contact forces obtained using the dynamic simulation.

Effect of the Track Curvature   A set of simulation results has been obtained with track curvatures ranging from 1.3 degrees to 9 degrees, a velocity of 5 m/s and zero superelevation. The simulation results show that for curvatures below 1.3 degrees the wheel set has only two points of contact. Figure 24 shows the yaw angle versus the track curvature. The plot shows the results obtained with the steady state equilibrium analysis and the dynamic simulation using the elastic and the hybrid methods. The agreement between the results of the specialized steady state formulation and the results of the forward dynamics simulations is good, especially when the hybrid method is used. Figure 25 shows the lateral force at the flange contact. Again, there is a good agreement between the results of the specialized steady state formulation and the results of the forward dynamics methods. Figures 26 shows the lateral forces at right tread. In general, the agreement between

12   Copyright © 2003 by ASME

the specialized steady state formulation and the hybrid method is better. This is expected since in the hybrid method the two tread contacts are modeled using constraints as in the case of the specialized steady state formulation. The differences between the results of the specialized steady state formulation and the results of the forward dynamics become more significant for high curvatures.
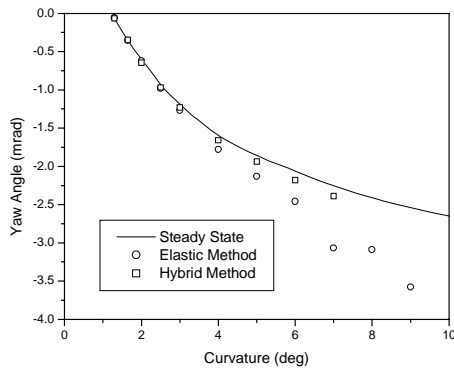

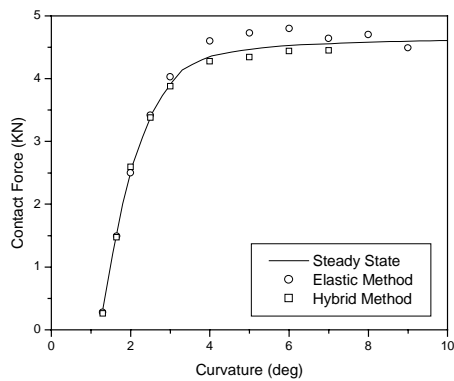Figure 24. Yaw angle (velocity 5 m/s, zero superelevation).

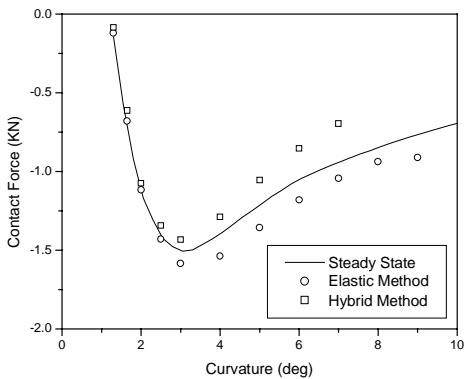Figure 25. Lateral force at the flange contact (velocity 5 m/s, zero superelevation).

Figure 26. Lateral force at the right tread contact(velocity 5 m/s, zero superelevation).

Influence of Track Superelevation A set of results have been obtained for superelevations ranging from 0 to 200% of the balanced superelevation, forward velocity of 5 m/s and a curvature of 5 degrees. Figure 27 shows the yaw angle as function of the superelevation. The absolute values of the yaw angle are larger in the case of forward dynamics, particularly in

the case of the elastic method. However, the rate of change shows a good agreement. Figure 28 shows the three contact forces, including normal contact forces and creep forces. Note that a large increase in superelevation leads to minor changes in the contact forces. The agreement between the results of the specialized the steady state formulation and the results of the hybrid forward dynamics method is again good.
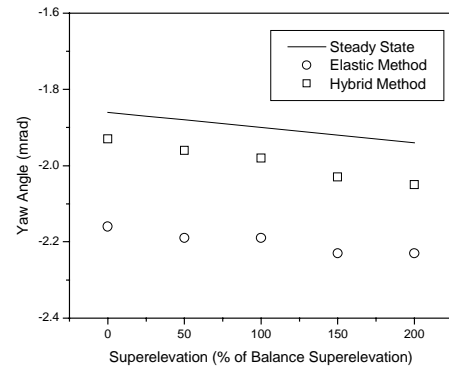
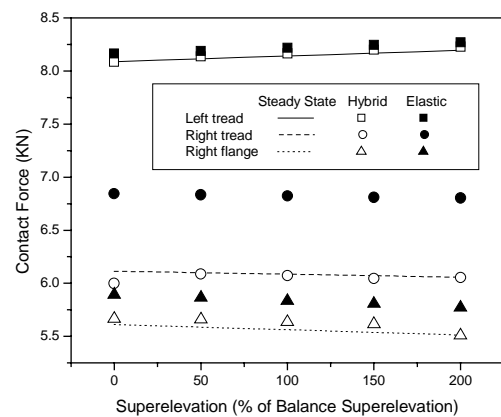

Figure 27. Yaw angle (velocity 5 m/s, curvature 5 deg).

Figure 28. Contact forces (velocity 5 m/s, curvature 5 deg).

7. SUMMARY AND CONCLUSIONS

This paper examines the steady state curving behavior of wheel sets traveling on a track with constant curvature. Using the steady state configurations obtained using the specialized formulation to test the performance of a multibody dynamic computer algorithm developed for railroad vehicles. The kinematic variables and contact forces obtained using the specialized steady state formulation are compared with the results of the inverse dynamics and forward dynamics multibody system formulations.

In the steady state configurations, the kinematics of the wheel set with three points of contact with the rail can be described using the yaw angle and the wheel set angular velocity about its axis. It has been shown that the wheel set has negative yaw angles for low forward velocities. The absolute value of the yaw angle decreases when the forward velocity increases, and the yaw angle becomes positive for large forward velocities. However, when the curvature of the track is varied, the absolute value of the yaw angle increases for low curvatures up to a maximum value. For larger curvatures, the absolute value of the yaw angle decreases. With regard to the

superelevation, it has been shown that the yaw angle increases as the superelevation increases. With regard to the normal contact forces, in general, the force on the left wheel (at the inner rail) decreases as the forward velocity or the curvature of the track increases, while the two forces on the right wheel (at the outer rail) increase. On the contrary, the force on the left wheel increases and the two forces on the right wheel decrease as the superelevation of the track increases. The comparison of the forces obtained using the specialized steady state formulation and those obtained using the general multibody dynamic equations show a good agreement. Both inverse dynamics and forward dynamics solutions show a good agreement with the steady state configurations predicted using the specialized wheel set formulation.

ACKNOWLEDGMENTS

REFERENCES

1. Nadal, M. J., "Locomotives a Vapeur", Collection Encyclopedie Scientifique, Biblioteque de Mecanique Appliquee et Genie, Vol. 186, Paris, 1908.
2. Elkins, J.A. and Weinstock, H., "The effect of two point contact on the curving behavior of railroad vehicles", ASME 82-WA/DSC-13.
3. Boockock, D., "Steady state motion of railway vehicles on curved track", *Journal of Mechanical Engineering Science*, **2**(6), 1969.
4. Elkins, J.A. and Gostling, R.J., "General quasi-static curving theory for railroad vehicles", in *Proceeding 5th VSD 2nd IUTAM Symposium*, Vienna, 1978, pp. 388-406.
5. Garg, V.K. and Dukkitapi, R.V., *Dynamics of Railway Vehicle Systems*, Academic Press, New York, 1988.
6. Nagurka, M.L., Bell, C.E., Hedrick, J.K. and Wormley, D.N., "Computational methods for rail vehicle steady-state curving analysis", *Computational Methods in Ground Transportation Vehicles*, AMD **50**, ASME/WAM, 1982.
7. Smith, K.R., MacMillan, R.D., and Martin, G.C., "2, 3 and 4 axle rigid truck curve negotiation model, technical manual", Research Report R-206 Association of American Railroads, Chicago, 1976.
8. Hedrick, J.K., Wormley, D.N., Arslan, A.V. and Chin, R., "Nonlinear analysis and design tools for rail vehicles: nonlinear locomotive dynamics", Research Report R-463, prepared for the Association of American Railroads, Chicago, by the Department of Mechanical Engineering, M.I.T., Massachusetts, 1980.
9. Dukkitapi, R.V. and Swamy S.N., "Non-linear steady-state curving analysis of some unconventional rail trucks", *Mechanism and Machine Theory*, **36**, 2001, pp. 507-521.
10. Meinke, P. and Blenkle C., "On the stability of narrow curving motion of railway wheelsets", *Machine Dynamics Problems*, **24**, 2000, pp. 131-136.
11. Shabana, A.A., Zaazaa, K.E., Escalona J.L. and Sany, J.R., "Dynamics of the wheel/rail contact using a new elastic force model", Technical Report # MBS02-3-UIC, Department of Mechanical Engineering, University of Illinois at Chicago, June, 2002.
12. Berzeri, M., Sany, R.J., and Shabana, A.A. "Curved track modeling using the absolute nodal coordinate formulation", Technical Report # MBS00-4-UIC, Department of Mechanical Engineering, The University of Illinois at Chicago, July 2000.
13. Kalker, J.J., "Survey of wheel-rail rolling contact theory", *Vehicle System Dynamics* **8**(4), 1979, 317-358.
14. Bödecker, C., "Die Wirkung zwischer rad und schiene", 1887.
15. Shabana, A.A., and Sany, J.R., "An augmented formulation for mechanical systems with non-generalized coordinates: application to rigid body contact problems", *Journal of Nonlinear Dynamics*, **24**, 2001, pp.183-204.
16. Shabana, A.A., *Computational Dynamics*, Second Edition, John Wiley & Sons, 2001.